RESEARCH

Investigations of Talbot and Talbot–Lau effects with various light sources

Sitti Buathong[1,2] · Sorakrai Srisuphaphon[1,2] · Pissunee Deechuen[1,2] · Nattawut Suksawat[1,2] · Kritsada Buasri[1,2] · Thanawee Chodjarusawad[1,2] · Sarayut Deachapunya[1,2,3]

Abstract

The near-field Talbot and Talbot–Lau effects have been performed with various light sources. First, a tunable diode laser in external cavity diode laser configuration for 483 nm has been used to check the theoretical framework utilized in these recent studies. An optical carpet is used to exhibit this result. Second, the Talbot effect with 635 nm light-emitting diode can be implemented with varied distances between the light-emitting diode and the grating. The results show that the Talbot effect can be achieved with monochromatic spatially incoherent light such as a light-emitting diode source, when using a long enough distance between the light-emitting diode and the grating. This makes it possible to avoid the complicated requirements for the Talbot–Lau effect. Third, in this section, an interesting phenomenon associated with the Talbot–Lau effect has been explored. The phase shift for each Talbot distance that normally occurs only in the Talbot effect can also be seen in Talbot–Lau if the second grating period is half that of the first grating. Also interference contrast gains in this configuration, which might be useful in optical applications. In the last section, we demonstrate an application from our recent studies. A wavemeter for measuring a spatially incoherent light source, such as a light-emitting diode or a fluorescent emitter, is one possible application. This study provides useful information on special optical techniques and their applications. Optical sensors with light-emitting diode in the Talbot configuration can be possible. Matter wave interferometric experiments also benefit if the contrast is higher in the Talbot–Lau effect with two gratings that have different periods.

1 Introduction

The discovery of the Talbot effect dates back by almost two-hundred years, when Henry Fox Talbot [1] shone a white light to a periodic grating and detected the repeated multi-colored light patterns that shared the shape of the grating at some specific distances. Lord Rayleigh [2] later explained the effect as repercussions of a Fresnel or near-field diffraction phenomenon of a highly coherent light beam, and the lensless self-images of the diffraction grating appear repeatedly at longitudinal intervals from the grating plane,

separated by so-called Talbot length L_T, which can be approximated using paraxial optics as D^2/λ, where D is the grating period and λ represents the wavelength of the optical source. Since then, numerous advancements related to this near-field effect have been reported. Spatial manifestation of the Talbot carpets, the optical carpets originated from integer, and fractional Talbot effects were demonstrated using a coherent optical source [3]. The light carpet was demonstrated to be capable of prime number decomposition [4]. Demonstrations of the Talbot effect associated with other optical elements including a mask grating, a lens, and a double-slit were examined [5–7]. High contrast Talbot patterns were obtained through an approach using two overlapping gratings [8]. It was also shown that an appropriate spherical wave front, formed via a monochromatic beam and a microscopic objective, could bring about the angular Talbot carpet in angular spectrum [9], where the phase of the angular Talbot carpet was later investigated using a far-field holography method [10]. The Talbot effect idea was extended to create temporal Talbot carpets, which could be produced by bright or dark pulse trains transmitted in dispersive optical

✉ Sarayut Deachapunya
sarayut@buu.ac.th

1 Department of Physics, Faculty of Science, Burapha University, Saen Suk, ChonBuri Province 20131, Thailand

2 Quantum and Nano Optics Research Unit, Burapha University, Saen Suk, ChonBuri Province 20131, Thailand

3 Thailand Center of Excellence in Physics, Ministry of Higher Education, Science, Research and Innovation, 328 Si Ayutthaya Road, Bangkok 10400, Thailand

components and observed in single-mode fibers [11, 12]. Using space-time wave packets, the temporal Talbot effect in free space [13] and the veiled space–time Talbot effect [14, 15] were achieved. The nonlinear Talbot phenomenon from nonlinear optical beams was explored experimentally and theoretically as well [16–18]. The Talbot patterns based on periodic structures of Bose–Einstein condensates [19, 20] and electromagnetic induced transparency atomic medium [21, 22] were formulated—displaying atom–light interactions. The Talbot sources are not only restricted to optical beams, but the effect was also demonstrated for ultrasonic and water waves [23, 24]. Moreover, the Talbot effect was applied in the production of an optical lattice [25], to the detection of diffraction grating period [26], spectral measurements [27–29], characterization of optical vortices with multiple topological charges [30–35], lithography processes [36], and to optical manipulation of minuscule particles [37].

The Talbot idea was also expanded by Lau for spatially incoherent sources using a double setup with same-period gratings, later named as the Talbot–Lau effect [38]. Incoming waves are made transversely coherent by the first grating and interfered to form the Fresnel diffraction patterns by the second grating [3, 39]. These patterns almost resemble those of the Talbot effect, except for having no lateral phase shifts of the self-images for odd multiples of the Talbot length. The Lau studies found applications in optical lithography and medical X-ray imaging. The Talbot–Lau fringes produced by light-emitting diode (LED) arrays were scrutinized for photolithography [40]. In medical imaging, X-ray Talbot–Lau phase-contrast interferometers were employed for detecting human organs [41, 42]. Recent techniques for X-ray Talbot–Lau interferometry involve enhanced phase gratings composed of gold [43], a scanning configuration which could picture large target samples [44], and mechanical systems that could adapt the Talbot–Lau setup to function for conventional X-ray imaging [45]. Due to de Broglie wave nature of incoherence, many works have also focused on matter wave interferometry based on the near-field Talbot–Lau effect to probe particle quantum properties [46, 47]. These near-field interferometers were used with various particles including rubidium atoms [48], fullerenes [49], positrons [50], oligoporphyrins [51], and antibiotic polypeptides [52]. The Talbot–Lau structure was proposed for inertial detection for particle beams [53]. The Talbot–Lau interferometer was used with a neutron beam and exploited for investigation of the inner frameworks of electrical steel sheets [54], magnetic field spatial distribution [55], and the splitting of the spin states [56].

In this paper, studies to further enrich our knowledge on the Talbot and Talbot–Lau effects for different types of spatially coherent and incoherent optical sources, such as a 483 nm external cavity diode laser, and a common single 635 nm LED, are reported. Talbot carpet weaved by the overlapping

grating method [8] and Talbot–Lau carpets fabricated via same- and different-period diffraction gratings were implemented. The characteristics of transverse phase shifts in the Talbot–Lau images with high clarity appeared when using a first grating having a period twice that of the second grating. Led by the results in these studies, the concept of a wavemeter for incoherent light is proposed as well.

2 Talbot effect with 483 nm tunable diode laser

First, we implement the optical carpet using the 483 nm tunable diode laser in the Talbot effect with two overlapping gratings. This laser source is an external cavity diode laser. Figure 1(a) schematically illustrates the set-up, consisting of a plane wave of light with wavelength λ diffracting through a grating G_1 by a distance L_1 to another grating G_2 having the same period D. The grating open fraction f provides a grating window size $a = fD$, such as $f = 0.5$ for a typical Ronchi grating. Adjusting the transverse shift δ provides a smaller open fraction f and can deliver an interference pattern with higher contrast behind the grating
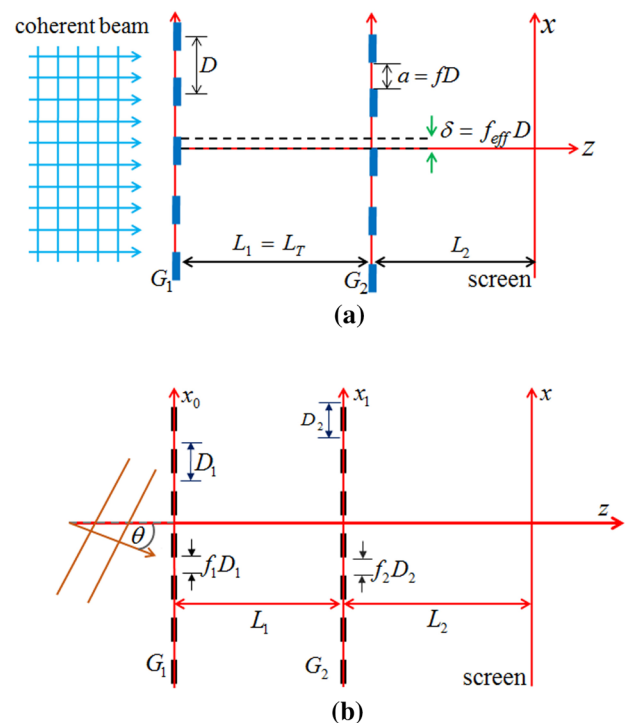

Fig. 1 **a** A coherent beam diffracts through the grating G_1. The first grating self-image of G_1 at $L_1 = L_T$ delivers another diffraction via G_2. A smaller open fraction of the Talbot pattern can be obtained by selecting an appropriate transverse shift δ. **b** An incoherent beam propagates through the Talbot–Lau setup with G_1 and G_2 to a screen along the x-axis over distances L_1 and L_2, respectively

G_2. The grating transmission function can be written as, $T_G(x_0) = \Sigma_n A_n \exp(2\pi i n x_0/D)$. Therefore, in the near-field regime with the Fresnel approximation, the exact wave function on the screen in Fig. 1(a) is given by [8]

$$\psi_1(x, L_1, L_2) = \sum_{n_1, n_2} A_{n_1} A_{n_2} \exp\left\{ \frac{2\pi i}{D}[(n_1 + n_2)x - n_2\delta] \right\}$$
$$\times \exp\left\{ \frac{i\pi\lambda}{D^2}[n_1^2 L_1 + (n_1 + n_2)^2 L_2] \right\},$$

(1)

where $A_{n_1} = \sin(n_1\pi f)/n_1\pi$, and $A_{n_2} = \sin(n_2\pi f)/n_2\pi$ are the Fourier component associated with the periodicity and the open fraction of grating [3]. At $L_1 = L_T$, the transverse shift δ equal to $f_{eff}d$ with $f_{eff} < 0.5$ is expected to provide a narrower effective open fraction as presented in Ref. [8]. Figure 2 illustrates a simulation of the optical carpet according to $I_1 = \psi_1^*\psi_1$ in comparison to the experimental results for $\lambda = 483$ nm with $D=100$ μm for both gratings (i.e., diffraction gratings with 10 lines/mm, PHYWE). The theoretical simulation matches the experiment when setting $f_{eff} \simeq 0.25$. The experiment can be set to this $f_{eff} \simeq 0.25$ by scanning the second grating G_2 transversely.

Our results confirmed that the method of overlapping gratings for small open fraction was able to create
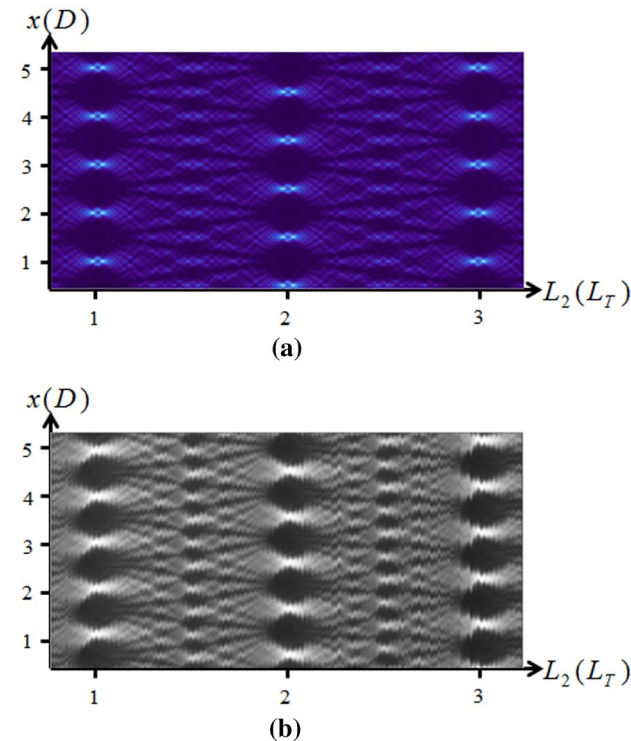

(a)

(b)

Fig. 2 Optical carpet generated with 483 nm tunable diode laser in two-grating Talbot setup for $0.76L_T < L_2 < 3.24L_T$ with 25 μm steps used in scanning, and $D=100$ μm: **a** simulation according to $I_1 = \psi_1^*\psi_1$, and **b** experiment. The effective open fraction was set as $f_{eff} \simeq 0.25$

high-contrast fractional and integer Talbot patterns [8, 57] comparable to those optical carpets formed by a single symmetric grating. The external cavity diode laser with a wavelength of 483 nm is essential for two-photon Rydberg excitation of rubidium atoms, which could be incorporated with electromagnetically induced Talbot carpet for optical imaging that provides a diagnostic tool for neutral atoms or molecules. This novel concept will be further tested in our laboratory in the near future.

3 Talbot effect with 635 nm light-emitting diode

We explore the implications of an incoherent and spherical wavefront to the near-field pattern. The incoming beam, from a LED, propagates along the z-axis with a wavefront on the x_0-axis (Fig. 3). For the spatial incoherent beam, we utilize an initial wave function $\psi_0(x_0) = \exp(ik_\theta x_0)$ where $k_\theta = k \sin\theta$ represents the projection of the incident wave vector ($k = 2\pi/\lambda$) onto the x_0-axis [3]. The spherical wavefront is considered by applying the transmission function $T_R(x_0) = \exp(-ikx_0^2/2R)$ with R representing a radius of curvature. Subsequently, the grating transmission function $T_G(x_0)$ is used to obtain a wave function behind the grating, G_1 (Fig. 3). Therefore, the diffracted wave function on the xz plane is obtained by applying the Huygens-Fresnel integral

$$\psi_2(x, z) = \hat{F}(x, z; x_0, 0) T_G(x_0) T_R(x_0) \psi_0(x_0).$$

(2)

Here, $\hat{F}(x, z; x_0, z_0)$ is assigned as a transition operator

$$\hat{F}(x_b, z_b; x_a, z_a) \equiv \sqrt{\frac{ik}{2\pi(z_b - z_a)}} e^{-ik(z_b - z_a)} \int_{-\infty}^{\infty} dx_a \, e^{\frac{-ik(x_b - x_a)^2}{2(z_b - z_a)}}.$$

(3)

The longitudinal positions (z_a and z_b) can be reduced to $z_a = 0$ and $z_b = z$, then $z_b - z_a = z$. The analytic calculation yields
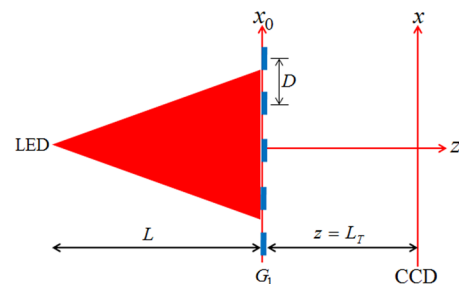

Fig. 3 Experimental Talbot setup for 635 LED with varied distances between LED and grating (L)

$$\psi_2(x,z) = \sum_n A_n \exp\left\{\frac{2\pi i n(x+z\sin\theta)}{MD} + \frac{i\pi n^2 z}{M(D^2/\lambda)}\right\}, \tag{4}$$

where the $M = 1 + (z/R)$ in the obtained expression can be interpreted as the magnification to the fringe period and the Talbot length, respectively. The factor constants including the phase constant were neglected.

The influence of spatial incoherence can be included by taking the sum over all θ contributing to the intensity [3],

$$I_2 = \sum_{\theta=-\pi/2}^{\pi/2} \psi_2^* \psi_2. \tag{5}$$

We use the approximation $\sin\theta \simeq \theta$ to replace the summation with an integral over small angles. Consequently, the calculation can be done analytically and yields

$$I_2' = \int_{-\theta_{max}}^{\theta_{max}} d\theta\, \psi_2^* \psi_2 = \sum_{n,m} A_n A_m \frac{MD}{\pi(n-m)z} \sin\left[\frac{2\pi(n-m)z\theta_{max}}{MD}\right]$$
$$\exp\left\{\frac{2\pi i(n-m)x)}{MD} + \frac{i\pi(n^2-m^2)z\lambda}{MD^2}\right\}, \tag{6}$$

where θ_{max} is less than 10 degrees to justify the approximation [58]. Lastly, the spectral bandwidth of the wavelength of the emitted light from the diode has to be involved. We assume a wavelength distribution following the Gaussian. Hence, the intensity pattern will be

$$I_2'' = \sum_{\lambda'=0}^{\infty} e^{-\frac{(\lambda'-\lambda)^2}{\sqrt{2}\beta^2}} I_2', \tag{7}$$

where β represents the radius of the wavelength distribution [59]. Figure 3 is a sketch of the setup. A LED with $\lambda = 635$nm was used as an incoherent source. The distance, L between the LED and the grating (G_1, $D = 100\mu m$, PHYWE) was varied, but the distance between the grating and the CCD camera (MT9J003 1/2.3-inch 10 Mp CMOS with pixel size p of 1.1 μm) was fixed as one Talbot length ($z = L_T$ =15.75 mm). The experimental results are shown in Fig. 4 for different distances L. The visibility of the pattern increases with distance as discussed above. In our recent experiment, the distance L larger than 300 mm, provides the starting of clear visibility. In Fig. 5, the theoretical simulations I_2'' match well the experimental results when fixing $\theta_{max} = 10^o$ and FWHM $\beta = 16\ nm = 2.5$ % of the center wavelength $\lambda = 635\ nm$. The magnifications $M = 1.40, 1.16, 1.07$, and 1.03 to match the extended interference fringes depend on the distances from the light source to the grating L.

The results in this section exhibit significant benefits as the Talbot effect can be applied even with spatially incoherent light if the distance from the light source to the grating
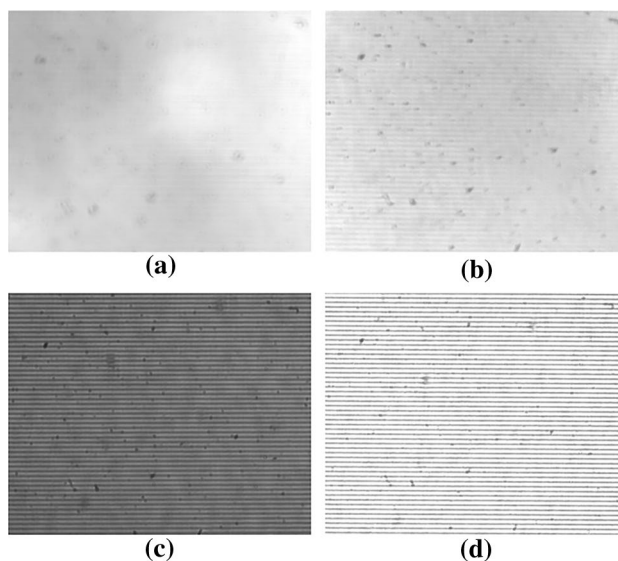
Fig. 4 Interference patterns in the Talbot setup with varied distances between LED and grating of **a** L= 30 mm, **b** 100 mm, **c** 300 mm, and **d** 500 mm. Visibility increases with the distance L

is large enough. One possible application is shown in the last section.

4 Talbot–Lau effect with 635 nm light-emitting diode

For this section, we consider the Talbot–Lau effect used an incoherent beam with two gratings. We employ the initial wave $\psi_0(x_0)$ with the wavenumber projection k_θ used in the previous section, but the light source is close to the grating. The wave diffracts through the grating G_1 to G_2, and these two gratings have periods (D_1, D_2), and open fractions (f_1, f_2), as depicted in Fig. 1(b).

According to the grating transmission function T_G and the defined transition operator Eq. (3), the wave function on the xL_2-plane is given by

$$\psi_3(x, L_1, L_2) = \hat{F}(x, L_2; x_1, 0)T_{G_2}(x_1)\hat{F}(x_1, L_1; x_0, 0)$$
$$T_{G_1}(x_0)\psi_0(x_0). \tag{8}$$

With analytic integrations, similar to Eq. (5), the intensity pattern including the spatial incoherence can be written as

$$I_3 = \sum_{\theta=-\pi/2}^{\pi/2} \psi_3^* \psi_3 = \sum_{n_1,n_2} \sum_{m_1,m_2} A_{n_1}(f_1) A_{n_2}(f_2) A_{m_1}(f_1) A_{m_2}(f_2)$$
$$\times \exp\left(iPx + iQ\lambda + iW\sin\theta\right), \tag{9}$$
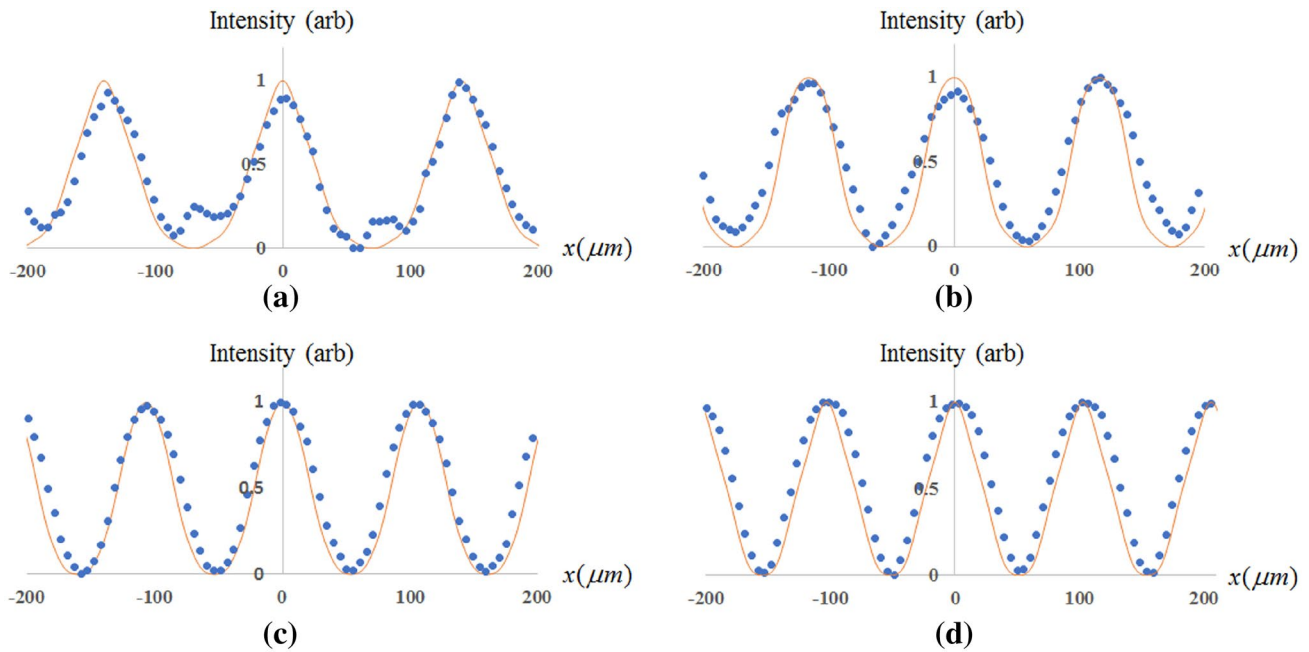
where

Fig. 5 The experimental interference patterns (the cross sections from Fig. 4) and the simulations (solid lines) according to Eq. (7) at $z = L_T$ =15.75 mm with $D = 100~\mu m$ and M=1.40 (**a**), 1.16 (**b**), 1.07 (**c**) and 1.03 (**d**). Please see the text for details

$$P = 2\pi\left(\frac{n_1 - m_1}{D_1} + \frac{n_2 - m_2}{D_2}\right), \tag{10}$$

$$Q = \frac{\pi L_1\left(n_1^2 - m_1^2\right)}{D_1^2} + \pi L_2\left(\left(\frac{n_1}{D_1} + \frac{n_2}{D_2}\right)^2 - \left(\frac{m_1}{D_1} + \frac{m_2}{D_2}\right)^2\right), \tag{11}$$

$$W = 2\pi\left(\frac{\left(L_1 + L_2\right)\left(n_1 - m_1\right)}{D_1} + \frac{L_2\left(n_2 - m_2\right)}{D_2}\right). \tag{12}$$

Using the small-angle approximation as in Eq. (6), we obtain

$$\begin{aligned}
I_3' &= \int_{-\theta_{max}}^{\theta_{max}} d\theta~\psi_3^*\psi_3 \\
&= \sum_{n_1,n_2,m_1,m_2} A_{n_1}A_{n_2}A_{m_1}A_{m_2}\frac{2\sin(W\theta_{max})}{W}e^{(iPx+iQ\lambda)}
\end{aligned} \tag{13}$$

However, the mixture of $k\sin\theta$ in each orientation results in the interference pattern disappearing unless the θ-dependence that corresponds to the factor $\sin(W\theta_{max})/W$ has a maximum value equal to 1 when W goes to zero. The vanishing of the function W is achieved under some particular conditions. As an example, in the case of $D_1 = D_2 = D$, the W will be zero only if

$$L_2 = L_1\frac{n_1 - m_1}{(m_1 - n_1) + (m_2 - n_2)}. \tag{14}$$

If we choose $L_1 = L_2 = L$, the function $W = 0$ in the series when $(n_2 - m_2) = -2(n_1 - m_1)$ [3] that makes $\sin(W\theta_{max})/W = 1$ and the exponent reduced to

$$iPx + iQ\lambda = \frac{2\pi i(m_1 - n_1)x}{D} + \frac{\pi i(m_1 - n_1)(m_2 + n_2)L}{D^2/\lambda}. \tag{15}$$

The above expression is similar to $\psi_1^*\psi_1$ (Eq.(1)), which can produce the optical carpet behind G_2 by maintaining $L_1 = L_2$. Not only the case $D_1 = D_2$ works, but also different grating periods can be used. For example, in the case $D_1 = 2D_2 = D$ with $L_1 = L_2$, the condition $W = 0$ is satisfied in the series when $n_2 - m_2 = m_1 - n_1$

$$iPx + iQ\lambda = \frac{2\pi i(m_1 - n_1)x}{D} + \frac{\pi i(m_1 - n_1)(m_2 + n_2)L}{2D^2/\lambda}. \tag{16}$$

The fraction 1/2 in the second term causes a longitudinal phase shift in the optical carpet compared to the typical case. Then, the theoretical simulations involving Gaussian wavelength distribution can be calculated as

$$I_3'' = \sum_{\lambda'=0}^{\infty} e^{-\frac{(\lambda'-\lambda)^2}{\sqrt{2}\rho^2}} I_3', \tag{17}$$

Our demonstration was done for these two cases, i.e., $D_1 = D_2 = 200~\mu m$ and $D_1 = 200~\mu m$, $D_2 = 100\mu m$, and the results are shown in Fig. 6. All gratings are binary grating with $f = 0.5$. The phase shifts (marked with the vertical

(a)
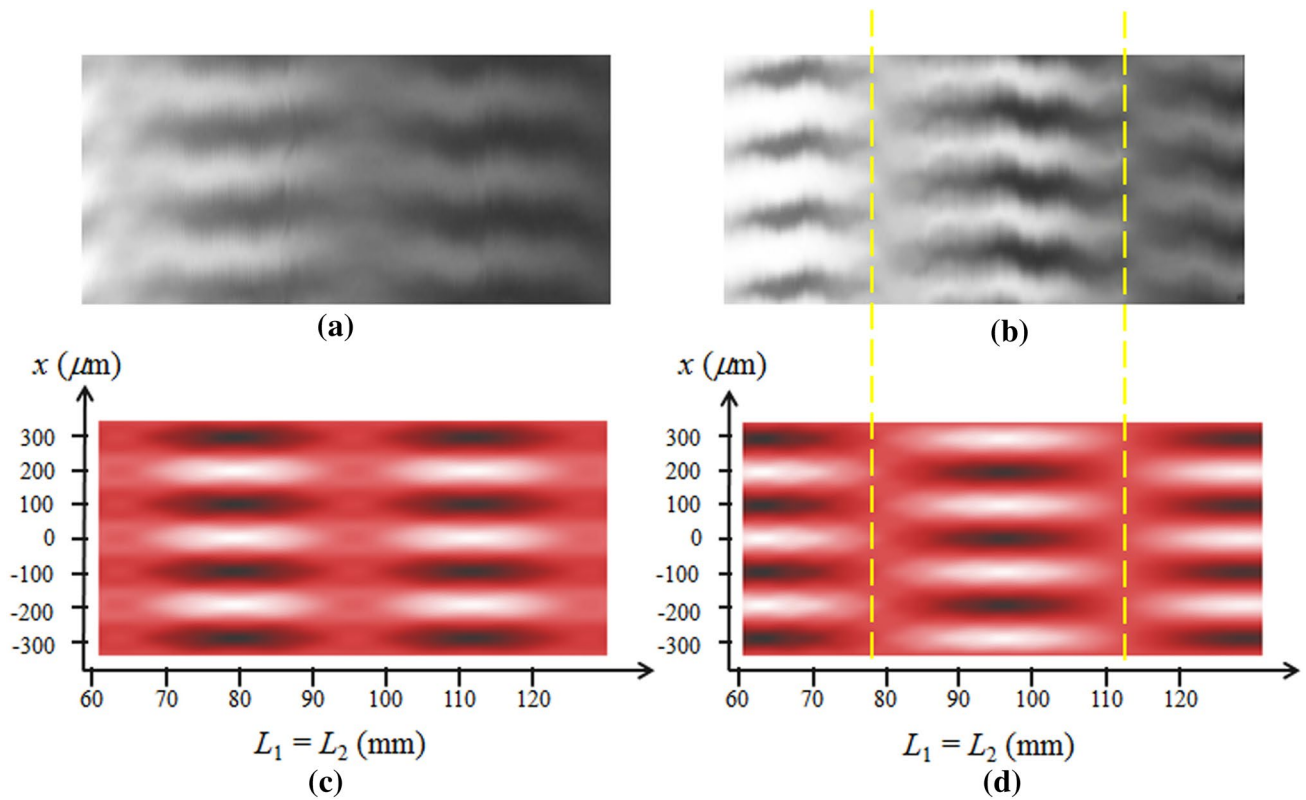
(b)

(c)

(d)

Fig. 6 Optical carpets of Talbot–Lau effect with $f_1 = f_2 = 0.5$ and **a** $D_1 = D_2 = 200\ \mu m$ (experiment with no phase shift), **b** $D_1 = 200\ \mu m$, $D_2 = 100\ \mu m$ (experiment with phase shift), **c** $D_1 = D_2 = 200\ \mu m$ (simulation (Eq. 17) with no phase shift), and **d** $D_1 = 200\ \mu m$, $D_2 = 100\ \mu m$ (simulation with phase shift). The vertical dashed lines mark the phase shift of the condition (**b**) and (**d**)

dashed lines) at Talbot distances, which typically occur only with the Talbot effect, can happen here with the condition that the second grating has half the period of the first grating. To the best of our knowledge, an appearance of this phase shift in the Talbot–Lau effect is here shown for the first time. Also, with this configuration, the interference contrast with at least twice the value can be clearly measured compared to a normal setup ($D_1 = D_2$). This makes benefit when working with low contrast sources such as in matter wave optics.

5 Application

A near-field Talbot wavemeter was earlier demonstrated with coherent light, such as a laser source [27, 28, 60, 61]. These schemes cannot be applied to spatially incoherent light sources. For these, a two-grating Talbot–Lau interferometer is required. We demonstrated the use of the Talbot effect with spatially incoherent light with the help of an optical fiber and a collimating lens [34]. The distance between the source and the grating must be large enough in order to obtain the interference pattern as presented in section 3. This can be satisfied using an optical fiber to stretch this length.

Our experimental setup, illustrated in Fig. 7(a), is suited for this purpose. It has a multi-mode fiber (MF, M42L01, Thorlabs) and lens (A390TM-B, Thorlabs) for adapting the incoherent light source to provide a transversely coherent wave. The inclined grating, G (80 Grooves/mm, Edmund optics) configuration can then generate an optical carpet which was detected by the camera (MT9J003 1/2.3-inch 10 Mp CMOS with pixel size p of 1.1 μm). In order to obtain the optical carpet, the periodicity of the grating must be aligned with the x-axis. Figure 7(b) and (c) represent the experimental optical carpets with a green light-emitting diode (LED) and a 780.24 nm tunable laser, respectively. Our tunable laser [62] with stable single-wavelength operation at around 780.24 nm (λ_{Cal}) was used for calibration. Therefore, the measured wavelength of an unknown light source (λ) can be extracted as

$$\lambda = \lambda_{Cal} L_{T(Cal)} / L_T, \tag{18}$$

where L_T and $L_{T(Cal)}$ are the Talbot lengths of the unknown light source and the calibrated laser (780.24 nm laser), respectively.

With this method, the empirical parameters, i.e., the grating period, the tilt angle (ϕ), and the camera pixel size, do
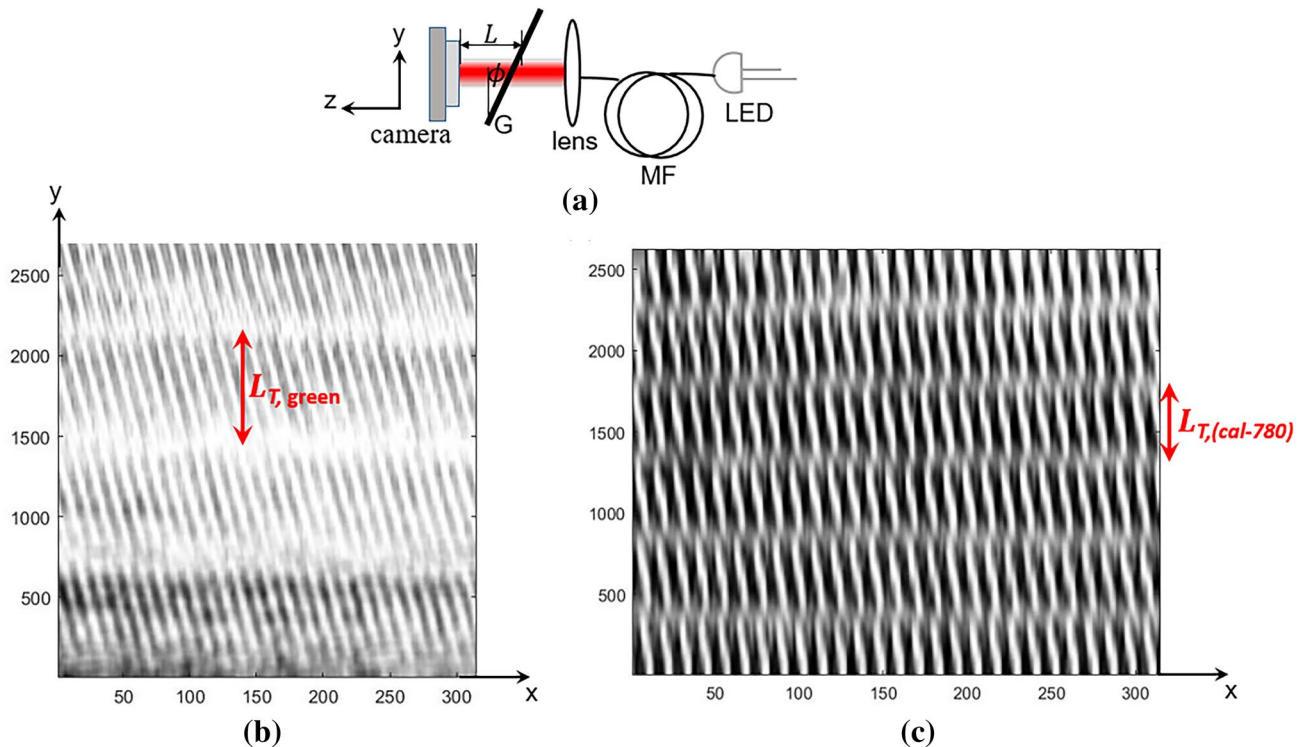
Fig. 7 Near-field wavemeter for incoherent light sources. **a** shows the experimental setup, while **b** and **c** are the optical carpets of green LED and calibration laser, respectively. The distance L from the grating to the camera was varied, allowing the optical carpet to be captured on a single image of the camera. Please see the text for details

not need to be known. According to our results, the wavelength of the green LED when calculated according to Eq. (18) was 535.92 nm. This is a typical value for this particular LED. The accuracy was based on that of the calibration laser.

6 Conclusion

Talbot and Talbot–Lau effects have a number of potential applications. In our work, a broadband spatially incoherent light can also be used for the Talbot effect, provided a long enough distance between the light source and the grating, for which an optical fiber can also be applied. In our example, the good contrast starts at the distance of about 300 mm. This is a good distance matching with the use of such fiber cables. Second, good interference contrast in the Talbot–Lau experiments can be gained if the second grating period is half that of the first grating. From our recent experiments, this contrast can be increased at least twice. In addition, the phase shift at each Talbot distance (which normally occurs only in the Talbot effect) can also be seen in this Talbot–Lau configuration. This observation might be useful in optics applications and even in matter wave optics. In the last section, a wavemeter for measuring a spatially incoherent light source has been demonstrated as one possible application. Our demonstration deals with the wavelength measurement of a green LED. The measured wavelength of 535.92 nm can be obtained nicely. We are convinced that our recent studies provide useful information to the optics community for both research and applications.

Author Contributions SB performed the experiments and wrote the manuscript. SS produced the theory and simulations and wrote the manuscript. PD, NS, KB, and TC performed the experiments. SD initiated the idea, performed the experiments, wrote, and finalized the manuscript.

Declarations

Conflict of interest The authors have no competing interests to declare that are relevant to the content of this article.

References

1. H.F. Talbot, Fact relating to optical science. Phi. Mag. Ser. **9**, 401–407 (1836)

2. J. Wen, Y. Zhang, M. Xiao, The Talbot effect: recent advances in classical optics, nonlinear optics, and quantum optics. Adv. Opt. Photonics **5**, 83–130 (2013)

3. W.B. Case, M. Tomandl, S. Deachapunya, M. Arndt, Realization of optical carpets in the Talbot and Talbot-Lau configurations. Opt. Express **17**(23), 20966–20974 (2009)

4. K. Pelka, J. Graf, T. Mehringer, J.V. Zanthier, Prime number decomposition using the Talbot effect. Opt. Express **26**, 15009–15014 (2018)

5. S. Deachapunya, S. Srisuphaphon, Sensitivity of transverse shift inside a double grating Talbot interferometer. Measurement **58**, 1–5 (2014)

6. S. Srisuphaphon, S. Deachapunya, The study of wave motion in the Talbot interferometer with a lens. Wave Motion **56**, 199–204 (2015)

7. W. Temnuch, S. Deachapunya, P. Panthong, S. Chiangga, S. Srisuphaphon, A simple description of near-field and far-field diffraction. Wave Motion **78**, 60–67 (2018)

8. S. Srisuphaphon, S. Buathong, S. Deachapunya, Simple technique for producing a 1D periodic intensity profile with a desired open fraction for optical sensor applications. J. Opt. Soc. Am. B **37**, 2021 (2020)

9. J. Azaña, H. Guillet de Chatellus, Angular Talbot effect. Phys. Rev. Lett. **112**(21), 213902 (2014)

10. H. Guillet de Chatellus et al., Phases of Talbot patterns in angular self-imaging. J. Opt. Soc. Am. A **32**, 1132–1139 (2015)

11. J. Wu, J. Hu, C.-S. Brès, Temporal Talbot effect of optical dark pulse trains. J Opt. Lett. **47**, 953–956 (2022)

12. B. Zheng, Q. Xie, C. Shu, Comb spacing multiplication enabled widely spaced flexible frequency comb generation. J. Lightwave Technol. **36**, 2651–2659 (2018)

13. L.A. Hall, S. Ponomarenko, A.F. Abouraddy, Temporal Talbot effect in free space. Opt. Lett. **46**, 3107–3110 (2021)

14. M. Yessenov, L.A. Hall, S.A. Ponomarenko, A.F. Abouraddy, Veiled Talbot Effect. Phys. Rev. Lett. **125**(24), 243901 (2020)

15. L.A. Hall, M. Yessenov, S.A. Ponomarenko, A.F. Abouraddy, The space-time Talbot effect. APL Photonics **6**, 056105 (2021)

16. Y. Zhang, J. Wen, S.N. Zhu, M. Xiao, Nonlinear Talbot Effect. Phys. Rev. Lett. **104**(18), 183901 (2010)

17. J. Wen, Y. Zhang, S.-N. Zhu, M. Xiao, Theory of nonlinear Talbot effect. J. Opt. Soc. Am. B **28**, 275–280 (2011)

18. Y. Zhang et al., Two-dimensional linear and nonlinear Talbot effect from rogue waves. Phys. Rev. E **91**(3), 032916 (2015)

19. C. Li et al., Optical Talbot carpet with atomic density gratings obtained by standing-wave manipulation. Phys. Rev. A **95**(3), 033821 (2017)

20. Y. Zhai et al., Talbot-enhanced, maximum-visibility imaging of condensate interference. Optica **5**, 80–85 (2018)

21. J. Wen, S. Du, H. Chen, M. Xiao, Electromagnetically induced Talbot effect. Appl. Phys. Lett. **98**, 081108 (2011)

22. J. Yuan et al., Integer and fractional electromagnetically induced Talbot effects in a ladder-type coherent atomic system. Opt. Express **27**, 92–101 (2019)

23. P. Candelas et al., Observation of ultrasonic Talbot effect in perforated plates. Ultrasonics **94**, 281–284 (2019)

24. A. Bakman, S. Fishman, Observation of the Talbot effect with water waves. Am. J. Phys. **87**, 38–43 (2019)

25. S. Deachapunya, S. Srisuphaphon, Accordion lattice based on the Talbot effect. Chin. Opt. Lett. **12**, 031101 (2014)

26. T. Photia et al., High-precision grating period measurement. Appl. Opt. **58**, 270–273 (2019)

27. E. Ye, A.H. Atabaki, N. Han, R.J. Ram, Miniature, sub-nanometer resolution Talbot spectrometer. Opt. Lett. **41**, 2434–2437 (2016)

28. N. Han et al., Compact and high-precision wavemeters using the Talbot effect and signal processing. Opt. Lett. **44**, 4187–4190 (2019)

29. Y. Li et al., A method to eliminate the matching problem and improve the spectral property of Talbot spectrometer. Opt. Lasers Eng. **148**, 106755 (2022)

30. P. Panthong et al., A study of optical vortices with the Talbot effect. J. Opt. **18**, 035602 (2016)

31. P. Panthong, S. Srisuphaphon, S. Chiangga, S. Deachapunya, High-contrast optical vortex detection using the Talbot effect. Appl. Opt. **57**, 1657 (2018)

32. D.A. Ikonnikov, S.A. Myslivets, M.N. Volochaev, V.G. Arkhipkin, A.M. Vyunishev, Two-dimensional Talbot effect of the optical vortices and their spatial evolution. Sci. Rep. **10**, 20315 (2020)

33. S. Buathong, S. Srisuphaphon, S. Deachapunya, Probing vortex beams based on Talbot effect with two overlapping gratings. J. Opt. **24**, 025602 (2022)

34. S. Srisuphaphon, S. Buathong, S. Deachapunya, Realization of an optical vortex from light-emitting diode source by a vortex half-wave retarder and using Talbot effect based detection. Opt. Laser Technol. **148**, 107746 (2022)

35. S. Deachapunya, S. Srisuphaphon, S. Buathong, Production of orbital angular momentum states of optical vortex beams using a vortex half-wave retarder with double-pass configuration. Sci. Rep. **12**, 6061 (2022)

36. P. Chausse, P. Shields, Spatial periodicities inside the Talbot effect: understanding, control and applications for lithography. Opt. Express **29**, 27628–27639 (2021)

37. E. Schonbrun et al., 3D interferometric optical tweezers using a single spatial light modulator. Opt. Express **13**, 3777–3786 (2005)

38. E. Lau, Beugungserscheinungen an Doppelrastern. Ann. Phys. (Leipzig) **437**, 417 (1948)

39. R. Sudol, B.J. Thompson, Lau effect: theory and experiment. Appl. Opt. **20**, 1107–1116 (1981)

40. X. Cao, P. Fesser, S. Sinzinger, Lau Effect Using LED Array for Lithography. Nanomanuf. Metrol. **4**, 165–174 (2021)

41. F. Horn et al., High-energy x-ray Talbot-Lau radiography of a human knee. Phys. Med. Biol. **62**(16), 6729–6745 (2017)

42. H. Yoshioka et al., Imaging evaluation of the cartilage in rheumatoid arthritis patients with an x-ray phase imaging apparatus based on Talbot-Lau interferometry. Sci. Rep. **10**, 6561 (2020)

43. J. Rieger et al., Optimization procedure for a Talbot-Lau x-ray phase-contrast imaging system. J. Instrum. **12**, 4018 (2017)

44. M. Seifert et al., Talbot-Lau x-ray phase-contrast setup for fast scanning of large samples. Sci. Rep. **9**, 4199 (2019)

45. N. Morimoto et al., Talbot-Lau interferometry-based x-ray imaging system with retractable and rotatable gratings for nondestructive testing. Rev. Sci. Instrum. **9**, 023706 (2020)

46. T. Juffmann et al., Wave and Particle in Molecular Interference Lithography. Phys. Rev. Lett. **103**, 263601 (2009)

47. K. Hornberger et al., Colloquium: Quantum interference of clusters and molecules. Rev. Mod. Phys. **84**, 157 (2012)

48. A. Turlapov, A. Tonyushkin, T. Sleator, Talbot-Lau effect for atomic de Broglie waves manipulated with light. Phys. Rev. A **71**, 043612 (2005)

49. B. Brezger, M. Arndt, A. Zeilinger, Concepts for near-field interferometers with large molecules. J. Opt. B **5**, S82 (2003)

50. S. Sala et al., First demonstration of antimatter wave interferometry. Sci. Adv. **5**, eaav7610 (2019)

51. Y.Y. Fein et al., Quantum superposition of molecules beyond 25 kDa. Nat. Phys. **15**, 1242–1245 (2019)

52. A. Shayeghi et al., Matter-wave interference of a native polypeptide. Nat. Commun. **15**, 1447 (2020)

53. S. Sala, M. Giammarchi, S. Olivares, Asymmetric Talbot-Lau interferometry for inertial sensing. Phys. Rev. A **94**, 033625 (2016)

54. T. Neuwirth et al., A high visibility talbot-Lau neutron grating interferometer to investigate stress-induced magnetic degradation in electrical steel. Sci. Rep. **10**, 1764 (2020)

55. J. Valsecchi et al., Visualization and quantification of inhomogeneous and anisotropic magnetic fields by polarized neutron grating interferometry. Nat. Commun. **10**, 3788 (2019)

56. J. Valsecchi et al., Decomposing Magnetic Dark-Field Contrast in Spin Analyzed Talbot-Lau Interferometry: A Stern-Gerlach Experiment without Spatial Beam Splitting. Phys. Rev. Lett. **126**, 070401 (2021)

57. D.V. Podanchuk et al., Adaptive wavefront sensor based on the Talbot phenomenon. Appl. Opt. **55**, B150–B157 (2016)

58. A. Goloborodko et al., Wavefront curvature restoration by a sensor based on the Talbot phenomenon under Gaussian illumination. J. Opt. Soc. Am. A **40**, B8–B14 (2023)

59. S. Deachapunya et al., Realization of the single photon Talbot effect with a spatial light modulator. Opt. Express **24**, 20029–20035 (2016)

60. H.L. Kung, A. Bhatnagar, D.A.B. Miller, Transform spectrometer based on measuring the periodicity of Talbot self-images. Opt. Lett. **26**, 1645–1647 (2001)

61. N. Guérineau, E.D. Mambro, J. Primot, F. Alves, Talbot experiment re-examined: study of the chromatic regime and application to spectrometry. Opt. Express **11**, 3310–3319 (2003)

62. W. Temnuch, S. Buathong, P. Phearivan, S. Deachapunya, Low-cost external cavity diode laser for cold atom experiments. J. Phys. **1719**, 012021 (2021)